



Published in final edited form as:

*J Phys D Appl Phys.* 2016 January 20; 49(2): . doi:10.1088/0022-3727/49/2/023001.

## Progress in Cherenkov femtosecond fiber lasers

Xiaomin Liu<sup>1</sup>, Ask S. Svane<sup>1</sup>, Jesper Lægsgaard<sup>1</sup>, Haohua Tu<sup>2</sup>, Stephen A. Boppart<sup>2</sup>, and Dmitry Turchinovich<sup>3</sup>

Xiaomin Liu: xali@fotonik.dtu.dk; Ask S. Svane: asksvane@gmail.com; Jesper Lægsgaard: jlag@fotonik.dtu.dk; Haohua Tu: htu@illinois.edu; Stephen A. Boppart: boppart@illinois.edu; Dmitry Turchinovich: turchino@mpip-mainz.mpg.de

<sup>1</sup>DTU Fotonik, Technical University of Denmark, DK-2800 Kgs. Lyngby, Denmark

<sup>2</sup>Biophotonics Imaging Laboratory, University of Illinois at Urbana-Champaign, Urbana, Illinois 61801, U.S.A

<sup>3</sup>Max Planck Institute for Polymer Research, Ackermannweg 10, 55128 Mainz, Germany

### Abstract

We review the recent developments in the field of ultrafast Cherenkov fiber lasers. Two essential properties of such laser systems – broad wavelength tunability and high efficiency of Cherenkov radiation wavelength conversion are discussed. The exceptional performance of the Cherenkov fiber laser systems are highlighted - dependent on the realization scheme, the Cherenkov lasers can generate the femtosecond output tunable across the entire visible and even the UV range, and for certain designs more than 40 % conversion efficiency from the pump to Cherenkov signal can be achieved. The femtosecond Cherenkov laser with all-fiber architecture is presented and discussed. Operating in the visible range, it delivers 100–200 fs wavelength-tunable pulses with multimilliwatt output power and exceptionally low noise figure an order of magnitude lower than the traditional wavelength tunable supercontinuum-based femtosecond sources. The applications for Cherenkov laser systems in practical biophotonics and biomedical applications, such as bio-imaging and microscopy, are discussed.

### Keywords

ultrafast lasers; photonic crystal fibers; ultrafast nonlinear optics

## 1. Background and introduction

Compact ultrafast pulsed laser sources, particularly tunable in the visible (VIS) and ultraviolet (UV) optical ranges, are in high demand for biophotonics and biomedical applications such as fluorescence spectroscopy, short-wavelength multiphoton microscopy, and fluorescence lifetime imaging microscopy [1].

Traditionally used widely-tunable ultrafast light sources are optical parametric oscillators (OPO) usually based on solid-state laser technology [2]. The OPOs readily provide the output with spectral coverage extending all the way from UV to the mid-infrared (MIR), with the output signal duration ranging from femtosecond (fs) pulses to continuous wave [3]. The OPO technology, which is cavity-based and relies on the mechanical readjustment for

wavelength tuning, although having many advantages, cannot provide ease of use of operation, and is also relatively costly.

The development of compact, stable, widely-tunable, maintenance-free femtosecond all-fiber lasers at low cost offers a very promising alternative to classical solid-state lasers, and drives the new directions in both fundamental research and practical applications. Importantly, biophotonics and biomedical imaging applications ideally require a compact, power-efficient, regularly stable, durable, and service-free ultrafast laser source, thus making fiber-based laser sources the obvious choice. The main current solutions for such a laser are the all-fiber supercontinuum (SC) laser sources [4], and tunable laser sources based on four-wave mixing (FWM) and frequency doubling [5]. The main advantages and drawbacks these technologies are as follows.

The all-fiber SC lasers have already been commercialized and can generate light covering the VIS and near-infrared (NIR) spectral range with a spectral brightness exceeding 1 mW/nm. The tunability is realized by spectral-domain slicing with a tunable narrow-band filter at the output of the laser. With nonsilica based materials, SC with much broader wavelength up to the MIR has been demonstrated [6]. The simple layout and construction of the very robust all-fiber design make SC sources attractive in many applications ranging from frequency comb production to advanced medical imaging [7]. However, due to inherently high noise figure, complex temporal pulse shape, and fiber lifetime issues, many practical applications are still out of reach for SC sources. Tunable laser sources based on FWM and frequency doubling are another option, and wavelength tunability across the visible (VIS) range has been realized [5]. However, such laser systems are quite complex and rely on bulk optics, including a second harmonic generation crystal and grating pairs used for pulse compression, which impair the environmental stability and robustness, thus compromising their use in practical applications.

In view of the above, a new ultrafast laser solution is needed, fulfilling the requirements for real-life practical applications such as: broad-range (ideally, continuous) tunability, low noise, compactness, durability, and ease of service-free operation. A promising new technology fulfilling all of the above requirements are ultrafast fiber lasers based on fiber-optic Cherenkov radiation (FOCR), which has been studied intensively in the past decade, with the number of publications on the topic increasing exponentially. FOCR technology allows one to generate femtosecond, spectrally-isolated output tunable in the range *from UV to infrared* from optical fibers pumped at standard laser wavelengths (e.g. by Ti:Sapphire, Yb- and Er-lasers), based on the relatively simple physical mechanism as discussed in this review.

In this paper, in Section 2 we describe the basic principles of FOCR. In Section 3 we review the current status and recent developments in tunable CR fiber laser systems. In Section 4 we discuss the applications of the FOCR laser systems in biophotonics and biomedical imaging, and the future prospects of this technology. Finally, in Section 5 we summarize the paper.

## 2. Principles of fiber-optic Cherenkov radiation

Traditionally, Cherenkov radiation (CR) is known as light that is produced by charged particles passing through a dielectric medium while travelling at speeds above the phase velocity of light in that medium [8]. For solitons propagating in optical fibers, it has been shown that the frequency shift between the soliton and the emitted dispersive wave has a formal analogy to the CR process in one dimension [9] [10] [11]. The FOCR, which is also termed as dispersive wave generation [11][12][13] or nonsolitonic radiation [14], is produced when the central wavelength of an input ultrafast pump pulse lies in the anomalous dispersion region of the nonlinear photonic crystal fiber (PCF) [13]. This radiation originates from the perturbation of a stable temporal soliton by the third- and higher-order fiber dispersion. The FOCR was first noticed in numerical simulations performed in the context of third-order dispersion [9], and its properties have been intensely studied since then [9][10] [12][14].

The generated FOCR wavelength is governed by a simple phase-matching condition which requires that the FOCR propagates at the same phase velocity as the soliton [10]. Below we will explain how this phase-matching condition allows one to predict the wavelength of the generated CR signal, and even its dynamics as a function of input peak power. If we call  $\beta(\omega)$  the frequency-dependent wave vector of the optical signal, a phase-matching condition governing the FOCR process can be derived based on the nonlinear Schrödinger equation (NLSE) [13]:

$$\Delta k = \beta(\omega) - \beta(\omega_p) - \beta_1(\omega_p)(\omega - \omega_p) - \gamma P_p = 0 \quad (1)$$

where  $\beta_1 = d\beta/d\omega$ ,  $\omega_p$  and  $P_p$  are the centre frequency and peak power of the soliton pulse, and  $\gamma$  is the fiber nonlinear coefficient. If we expand  $\beta(\omega)$  in a Taylor series around  $\omega_p$ , the phase-matching condition can be expressed as:

$$\sum_{m=2}^{\infty} \frac{\beta_m(\omega_p)}{m!} \Omega^m = \gamma P_p \quad (2)$$

where  $\Omega = \omega - \omega_p$  is the frequency shift. To simplify the illustration, we only consider the third-order dispersion term, and ignore all the other higher-order terms. The resulting cubic polynomial  $\beta_3(\omega_p)\Omega^3 + 3\beta_2(\omega_p)\Omega^2 - 6\gamma P_p = 0$ , provides the following approximate solution [10]:

$$\Omega \approx -\frac{3\beta_2(\omega_p)}{\beta_3} + \frac{2\gamma P_p \beta_3(\omega_p)}{3\beta_2^2(\omega_p)} \quad (3)$$

When solitons propagate in the spectral region with anomalous dispersion  $\beta_2(\omega_p) < 0$  but with positive third-order dispersion  $\beta_3(\omega_p) > 0$ , the frequency shift  $\Omega$  is positive, which means that the FOCR is emitted at a higher frequency (shorter wavelength) than that of the soliton. With appropriate fiber parameters, a standard photonic crystal fiber (PCF) such as the one shown in the inset of Fig. 1(a), is capable of satisfying this condition over wide wavelength ranges [15].

One calculated example of FOCR emission in the PCF is shown in Fig. 1. A 230 fs pump pulse at 1030 nm central wavelength with 8 kW peak power was simulated to propagate through the PCF. The peak power and spectral evolution of the pump pulse propagation along the PCF are plotted in Fig. 1(a) and (b), respectively. The red line in Fig. 1(b) shows the dispersion profile of the PCF, which has a zero-dispersion wavelength (ZDW) of 850 nm. As one can see, the pump signal initially undergoes nonlinear pulse compression due to the combination of the self-phase modulation (SPM) and anomalous dispersion of the PCF, resulting in the pump pulse peak power increasing and spectrum broadening. Around the point of maximal compression at 39 mm propagation length, when the peak power increases to ~ 89 kW, i.e. by more than one order of magnitude as compared to input, the visible FOCR pulses at 610 nm are generated. After the initial compression point, recurring recompression occurs as the pump decreases in peak power along the propagation length.

As follows from Eqs. (1) and (2), the phase-matching condition involving the pump source and its resonant CR allows one to predict the FOCR wavelength based on the dispersion profile of the propagation fiber [16]. The great structural flexibility makes the optical properties of PCFs such as dispersion and nonlinearity more designable and controllable as compared to standard optical fibers. As an example, Fig. 2 (a) shows the calculated group velocity dispersion profiles for four PCF designs having  $d/\Lambda = 0.9$  which have normally been used for FOCR generation, based on the method described in [17]. Here  $d$  is the PCF airhole diameter and  $\Lambda$  is the PCF pitch - the center-to-center distance between neighboring airholes. When the fiber pitch  $\Lambda$  is scaled down from 3  $\mu\text{m}$  to 1.5  $\mu\text{m}$ , ZDW of the PCF is blue-shifting from 850 nm to 670 nm.

When the contribution of the nonlinear term in Eq. (1) is negligible, the linear FOCR phase match can be calculated by finding fully vectorial eigenmodes of Maxwell's equations with periodic boundary conditions in a planewave basis using the freely available software package 'MIT Photonic-Bands' [18]. The calculated phase-matching curves for four fiber designs having  $d/\Lambda = 0.9$  with the pump wavelength of 1033 nm are shown in Fig. 2(b). A phase-matching region in the VIS region around 400–600 nm can be obtained by scaling the pitch  $\Lambda$  in the range between 1.5 - 3  $\mu\text{m}$ . When reducing  $\Lambda$ , the linear FOCR phase-matching wavelength shifts to shorter wavelengths. If the non-linear FOCR phase-matching, corresponding to the term  $\gamma P_P$  from Eq. (1), is considered, phase-matching point shifts to slightly positive values of  $k$  as shown in Fig. 2(b). This leads to certain degree of FOCR wavelength tunability: an increasing blue-shift in the FOCR phase-matching wavelength is expected for the increasing pulse powers.

Fig. 3(a) shows the ZDW (dashed line) as well as the linear FOCR phase-matching (solid line) for a 1033 nm pump wavelength as a function of the PCF fiber pitch, with  $d/\Lambda = 0.9$ . When reducing the fiber pitch, both the ZDW and FOCR wavelengths acquire blue-shift. The FOCR wavelength can cover all the visible range and even extend down to the UV, when the ZDWs of the PCFs shift from around 850 to 670 nm, which can be realized by a series of commercially-available PCFs. As follows from Eqs. (1, 2), besides the fiber properties, the FOCR wavelength is also dependent on the pump wavelength. Fig. 3(b) shows the predicted linear FOCR phase-matching wavelength with two different pump wavelengths around 1  $\mu\text{m}$  and 1.55  $\mu\text{m}$ , characteristic of standard modelocked Yb- and Er-

fiber lasers. When the pump wavelength is further away from the ZDW of the PCF, an even shorter FOCR wavelength can be generated.

Importantly, in general FOCR can be generated at *both shorter and longer wavelengths* with respect to the pump pulse: this is governed by the fiber dispersion profile, especially by the third-order dispersion  $\beta_3$ , at the pump wavelength (see Eq. 3). The discussion above concerns the *frequency up-conversion* of FOCR from the pump signal (the FOCR frequency is higher than the pump signal frequency), which is the case when the PCF has a dispersion profile such that  $\beta_2(\omega_p) < 0$  and  $\beta_3(\omega_p) > 0$  at pump signal wavelength (see Eq. 3). On the other hand, a *frequency down-converted* FOCR can be generated if  $\beta_2(\omega_p) < 0$  and  $\beta_3(\omega_p) < 0$  at pump signal wavelength. Possibility to both up- and down-convert the pump laser light provides the great opportunity for FOCR technology, leading to ultrafast fiber lasers with the output covering the range from UV to infrared.

### 3. Current progress in fiber-optic Cherenkov radiation

In this section, we provide an overview of the progress in the generation of fiber-optic Cherenkov radiation. The FOCR wavelength tunability and wavelength conversion efficiency, two essential properties of Cherenkov laser systems, are reviewed in Subsection 3.1 and 3.2, respectively. Finally, the demonstration of CR laser system in all-fiber, fully monolithic architecture, allowing a certain degree of electrical wavelength tunability, is discussed in Subsection 3.3.

#### 3.1. Widely tunable FOCR laser systems based on standard Ti:Sapphire, Yb-, and Er-laser pumping

Over the last decade, FOCR has emerged as a new wavelength-conversion technique to generate ultrafast pulses in the VIS, UV, and even the mid-IR wavelength range, where standard mode-locked fs lasers are not available. The state-of-the-art in FOCR generation is summarized in Table 1, and below we discuss selected achievements in the field.

In 2004, the groups of Degiorgio and Zheltikov demonstrated a VIS CR signal generated via the simple fiber-pumping procedure [13][20]. In 2006 Zheltikov *et al.* generated FOCR from birefringent PCFs to frequency up-convert the 820 nm and 1.24  $\mu\text{m}$  pump wavelengths into the visible region [21]. These experiments have also shown a certain degree of wavelength tunability, however only limited to 20 nm tuning range.

Meanwhile, the groups of Knox and Bernardo introduced submillimeter-scale dispersion micromanagement into a short (5–10 mm) PCF to generate femtosecond visible pulses from a Ti:sapphire laser [22][23]. In Ref. [24], tunable FOCR in the VIS range of 385–625 nm was generated by using a dedicated fiber-tapering technique to prepare a series of PCFs with different dispersion designs.

Tu *et al.*, using a  $\sim 1 \mu\text{m}$  pump source, have demonstrated that the PCF-generated CR can have an even broader tunability in the VIS down to the UV range, at multimilliwatt-level average output power. The FOCR central wavelength was tuned either by varying the pump wavelength of the femtosecond source laser [25] or by switching between the PCFs with

different dispersion properties [1][26][27]. In the work [25], multimilliwatt fundamental-mode FOCR signals tunable across 485–690 nm were generated from two dispersion-engineered PCFs. The signal wavelength was tuned by varying the pump wavelength of a modelocked Ti:sapphire laser, resulting in a wide tuning range of 690–1020 nm. Later, the FOCR with even broader wavelength tunability of more than 300 nm was demonstrated [1][26][27]. Conveniently, in these works neither the special dispersion engineering [24] nor the tuning of the pump wavelength [25] was necessary for the FOCR generation. By fixing the pump wavelength at 1020 nm with average power of 54–250 mW, the FOCR signals tunable across the range 347–680 nm from one series of PCFs were generated, as shown in Fig. 4(a). The generated FOCR spectrum from each fiber exhibits a single Gaussian-shaped band with the 3 dB bandwidth of 15 nm and an average power of a few milliwatts, and the far-field images of the generated FOCR are shown as the insets of Fig. 4(a). The PCFs used here all have similar structural cross-sections as shown in Fig. 4(b), while core sizes and ZDWs were varying. The dependence of the generated FOCR wavelength as a function of PCFs with varying ZDWs is shown in Fig. 4(c), perfectly following the theoretical prediction based on Eqs. (1–3).

More recently, tunable ultrafast FOCR pulses even in the deep-UV regime have been demonstrated. The Russell group reported tunable FOCR in the range of 176–550 nm generated in a gas-filled hollow-core photonic crystal fiber (HC-PCF), based on 800 nm pumping [28][29][30], as shown in Fig. 5. By careful optimization and appropriate choice of gas, assisted by detailed numerical simulations, the FOCR can be continuously tuned from 200 nm to 275 nm in Ar gas, and further extended to beyond 550 nm using Kr or Xe gas. FOCR pulse energies of more than 75 nJ were generated from 800 nm pump pulses of a few  $\mu$ J energy.

Due to the large optical frequency up-conversion ratio, equivalent to third (or fourth) harmonic generation, the  $\sim$ 1550 nm pump wavelength (Er-fiber laser) has not been used to generate the FOCR in the VIS and UV region in the fundamental mode of a silica-based fiber [31]. All the FOCR results listed above were achieved using near-infrared (NIR) laser sources with the center wavelength around 800 nm or 1  $\mu$ m. However, in the recent work by Tu *et al.* [31], FOCR wavelength conversion from the 1550 nm band of a fs Er-fiber laser has been realized. Using different nonlinear fibers with different dispersion and nonlinearity properties, the tunable FOCR throughout 370–850 nm range, corresponding to a blue-shift of 700–1180 nm, was generated, as shown in Fig. 6. In comparison to the fs Yb-fiber platform, the Er platform has the advantage that anomalous dispersion at the pump wavelength can be achieved in large-core fibers, thus facilitating FOCR power scaling to build more robust FOCR sources.

### 3.2. FOCR systems with high conversion efficiency

Besides the FOCR wavelength tunability range, the FOCR wavelength conversion efficiency is of equal importance [32][33][34] [35]. In Refs. [32][34][35] the pump-to-CR power conversion efficiency of more than 40% has been achieved (see Table 1).

In 2010, the Kärtner group investigated the dependence of FOCR conversion efficiency on the NIR pump pulse parameters (such as duration and pulse energy) and pulse evolution

along the propagation distance in the fiber [32]. As the simulations in Fig. 7 (a) show, highly efficient FOCR with conversion efficiency exceeding 40% in the VIS wavelength range, and an isolated spectrum spanning more than 60 nm can be achieved. Here a Ti:Sapphire laser emitting 10 fs, 300 pJ pulses is chosen as the pump source, to excite the FOCR-emitting PCF with ZDW at 710 nm, and 2 cm length. Fig. 7(b) illustrates calculated CR efficiency as a function of input pulse energy for three different pulse durations in the range 10 – 100 fs at FWHM. The results clearly suggest that CR generation efficiency can even exceed 40%, if few-cycle pump pulses are employed.

In Ref. [36], also by the Kärtner group, the FOCR generation in the few-cycle regime has been studied both theoretically and experimentally. In this work, three characteristic propagation scales were identified: 1) an initial buildup stage in which FOCR acquires most (>90%) of its energy; 2) quasi-independent propagation of FOCR with minimal interaction with its host soliton; and 3) strong interaction with the host soliton that is decelerated by stimulated Raman scattering (SRS). While the last SRS stage has been well studied before, the understanding of the first two stages in FOCR constituted a breakthrough contribution in understanding of FOCR dynamics.

Recently, Zhang *et al.* demonstrated the generation of highly efficient FOCR in the fundamental mode of a GeO<sub>2</sub>-doped PCF with two zero dispersion wavelengths [34]. Using a high power femtosecond Yb-doped PCF laser emitting 100 fs pulses as the pump source, FOCR with conversion efficiency of >40% and bandwidth of 38 nm was obtained in the VIS wavelength range when the average power of the pump light was 1.27 W. Such an efficient FOCR generation was achieved by injecting the pump light in the deep anomalous dispersion range of the PCF.

Based on the Kärtner group work by Chang *et al.* [32], in 2014 Chan *et al.* reported FOCR with record-high average output power (>250 mW), high pulse energy (>4 nJ), and excellent power conversion efficiency (>40%) from the PCF pumped by a 1.03 μm air-cooled Yb femtosecond laser [35]. Power-dependent output characteristics of the FOCR source with different PCF lengths were also measured and analyzed. The wavelength tunability of FOCR was realized by adjusting the pump power coupled into the PCF (see Fig. 2(b) and corresponding discussion in Section 2).

Since the first report of the PCF [37], most published research has been focused on the PCFs made of silica, as the silica-based fiber technology has been developed to a very mature state compared to other material alternatives. All of the FOCR work described above in this article has been done with silica-based PCFs. However, mid-infrared (MIR) wavelengths longer than 2.4 μm are difficult to access by using conventional silica glass fibers due to the strongly increasing losses in this spectral range [38]. These limitations can be overcome by moving to nonsilica glasses such as soft-glass fibers. Indeed, soft-glass microstructured optical fibers (MOFs), fabricated from tellurite or chalcogenide glasses, have broad transparency spectral window in the mid-IR, and high nonlinear refractive indices exceeding that of silica glass by at least one order of magnitude.

Most recently, Cheng *et al.* reported extremely high conversion efficiency of FOCR over 65% with a four-hole tellurite microstructured optical fiber (TMOF) [39]. The calculated fundamental mode refractive index and dispersion curve of the TMOF with  $\sim 4.7$   $\mu\text{m}$  core diameter are shown in Figs. 8(a,b). The ZDW of the TMOF is  $\sim 1720$  nm. The highly efficient FOCR generation in a 2-cm long TMOF with  $\sim 560$  fs pump signal at 1760 nm central wavelength is shown in Fig. 8(c). The center wavelength of the emitted FOCR is shifting from 1685 nm to 1626 nm as the pump power is increasing from 250 mW to 440 mW, and the conversion efficiency grows monotonously with the input pump power, reaching impressive 67.4% at  $\sim 495$  mW. There are two potential reasons to explain such a very high efficiency of FOCR generation demonstrated in this work [39]. One is the high nonlinear refractive index of the tellurite glass as compared to silica glass. As a result, the nonlinear term  $\gamma P_p$  in Eqs. (1–3) will be large, and accordingly the FOCR phase-matching condition can be satisfied in a relatively wide wavelength range. The other reason is the proximity of the pump wavelength to the ZDW of the TMOF, which means that the dispersion term of Eq. (2) is nearly zero. As a result, the FOCR phase-matching condition can be satisfied with the low pump power, as the pump pulse will maintain its peak intensity over a longer propagation distance.

### 3.3. All-fiber architecture of femtosecond FOCR laser system

For practical biophotonics and biomedical imaging applications, laser systems in all-fiber format are most desirable due the strong requirement on operational and environmental stability, and service-free laser operation. The FOCR laser systems described above largely rely on using bulk optics and free-space optical coupling to the fibers, and hence the achieved spectral agility and wide tunable spectral range are achieved to a certain extent at the expense of the system operational stability. On the other hand, the modelocked lasers with monolithic all-fiber architecture, such as e.g. [42][43], offer exceptional operational and environmental stability combined with the fiber-end femtosecond pulse delivery, clearly advantageous for real-life applications. To this end, an all-fiber system based on a Yb-fiber femtosecond laser, producing *electrically tunable* femtosecond FOCR output in the VIS spectral range with average power in the milliwatt range has been recently developed.

The layout of such an all-fiber fs CR laser system is shown in Fig. 9. The system is constructed of two key parts: an all-fiber fs pump source, and a spliced-on nonlinear CR fiber link [40]. All the fibers in the entire system are spliced together, and the polarization-maintaining (PM) fibers are used throughout the entire system where appropriate. The all-fiber pump source is a nJ-level self-stabilized Yb-fiber femtosecond master oscillator - power amplifier (MOPA) at a central wavelength of 1035 nm, with 28 MHz repetition rate. The details of the passively self-stabilized pump source can be found in [41][42][43].

Fig. 10(a) shows the typical output spectrum of the pump pulse with 10 nm full width at half maximum (FWHM) bandwidth. As is typical for all-fiber MOPAs, the pump pulse has a spectral structure and the temporal profile indicative of self-phase modulation and uncompensated higher-order dispersion. Nevertheless, as described below, even using such an “unclean” pump pulse, the FOCR with smoother spectrum and of shorter duration can be

generated. This emphasizes the robustness of FOCR process towards non-ideal pumping condition, which is in stark contrast to e.g. optical parametric generation.

The monolithic FOCR laser system uses spliced-together nonlinear fiber, consisting of one 10 cm small-core nonlinear PCF NL-3.0-850 (NKT Photonics A/S) with the ZDW around 850 nm for FOCR generation, and two bridge fibers with lengths of 2 mm and 8 cm, respectively. The pump pulses are delivered to the nonlinear link from the hollow-core PCF (HC-PCF) acting as a pulse compressor in the pump Yb-fiber MOPA. The mode-field diameters (MFDs) of the FOCR-generating NL-3.0-850 fiber, two bridge fibers, and the pump pulse compressor HC-PCF are 1.8  $\mu\text{m}$ , 3.3  $\mu\text{m}$ , 6.6  $\mu\text{m}$ , and 7.5  $\mu\text{m}$ , respectively. The use of two bridge fibers therefore provides a gradual reduction of MFD between the HC-PCF and the FOCR-generating NL-3.0-850 fiber. As a result, the total coupling loss in such a fiber link is only around 4 dB instead of 12 dB, which would result from splicing the HC-PCF and the FOCR-generating NL-3.0-850 fiber directly.

When fully compressed, the pump pulses propagating in the NL-3.0-850 fiber had an autocorrelation (AC) FWHM of 420 fs, as shown in Fig. 10(b). We note that the dispersion of the two bridge fibers used in the fiber link was normal at the pump wavelength. Therefore, for dispersion compensation, the pump pulses had to be negatively pre-chirped with group delay dispersion of  $-1.46 \cdot 10^4 \text{ fs}^2$  in order to provide the shortest pulse duration, and hence the highest peak intensity, while in the FOCR-generating NL-3.0-850 fiber.

The FOCR phase-matching condition implies that the peak power of the pump pulse is one of the key parameters determining the generated FOCR wavelength (see Fig. 1). In the experiments, the central wavelength of the emitted FOCR was shifting from 630 nm to 580 nm, yielding the blueshift as expected in this process [32], when the pump power was increasing from 130 mW to 330 mW. This spectral tunability is based on the control of the chirp and bandwidth of the pump signal by controlling the inversion in the amplifier section of the all-fiber pump laser [44]. The inversion is simply controlled by tuning the drive current of the pumping diode for the amplifier, thus bringing about the convenient *electrical* tunability of the FOCR central wavelength. As shown in Fig. 11(a), when the input pump power increases, the FWHM bandwidth of the emitted FOCR also increases correspondingly, from 14 nm to 36 nm, as driven by the Raman-induced redshift effect of the pump pulses.

The emitted FOCR power as a function of the input pump power is shown as blue symbols in Fig. 12(a). The generation threshold of the FOCR is around the pump power of 130 mW. After exceeding the generation threshold, the FOCR conversion efficiency grows significantly until the pump power reaches 180 mW, at which point the FOCR output starts to saturate. The output power range of 1 - 2.5 mW corresponds to pulse energies of 37 - 93 pJ. Such energies are high enough for practical biophotonic and biomedical imaging applications, and are comparable to those used in previously published 2-photon fluorescence microscopy experiments relying on filtered fiber supercontinuum (SC) [45] [46].

As we already mentioned in the introduction, both the all-fiber CR lasers and the all-fiber ps-SC sources are particularly intended for real-life practical biophotonics and biomedical imaging applications. The sensitivity of bio-imaging and microscopy systems, which is one of the key parameters for the performance evaluation of an imaging platform, is typically limited by the intensity noise of the laser source used in the system [47]. Therefore, it is essential to compare the noise properties of both types of such laser sources using the standard methods as described in Refs. [48], [49], [50]. The standard all-fiber ps-SC source used in this experiment for comparison is based on an Yb-fiber pump MOPA with a repetition rate of 80 MHz, spectrally sliced with a 10 nm bandwidth (FWHM) optical bandpass filter with the central wavelength around 600 nm [51][52]. The details of the noise measurements can be found in Ref. [53].

The noise of the all-fiber CR laser can be divided into two contributions: a low-frequency part originating from technical laser noise, and a broadband frequency part originating from amplified quantum noise [54], [55]. In particular, the low-frequency component of the intensity noise results mainly from the amplification of the input noise of the pump laser. The broadband frequency component of the intensity noise at the electrical frequency above 1 MHz arises from the two fundamental quantum noise seeds: the input shot noise, and spontaneous Raman scattering along the PCF fiber [55]. For primary applications of FOCR sources, such as nonlinear microscopy, the low-frequency noise part can be removed by high-frequency modulation of the excitation beam along with lock-in detection of the signal. With this arrangement, only the broadband frequency noise part contributes to the pulse-to-pulse fluctuations, which is investigated in work [53]. Relative intensity noise (RIN), a figure of merit of intensity noise characteristics, is quantified by the noise power in a 1 Hz bandwidth normalized to the DC signal power [49]. The pulse-to-pulse energy fluctuations can be calculated as a square root of the RIN integrated in frequency from a certain frequency and up to half the repetition rate [56]. The signal-to-noise ratio (SNR) is then defined as the reciprocal of the pulse-to-pulse energy fluctuations.

The red symbols in Fig. 13(a) show the SNR of the all-fiber CR laser as a function of the input pump power. The SNR of FOCR increases to 40.4, corresponding to a pulse energy fluctuation as low as 2.48%, when the average output power reaches 4.3 mW. For comparison, Fig. 13(b) shows the SNR of the 10 nm-wide spectrally filtered output of the ps-SC at 600 nm central wavelength, as function of input pump power. The ps-SC source shows a peak SNR of only 3.48, corresponding to pulse energy fluctuations as high as 28.78%, when the pump power reaches 10 W. The SNR of our all-fiber CR source is found to be 10.6 dB better than that of the measured ps-SC source operating at the same wavelength. The 10.6 dB difference in SNR between the FOCR and ps-SC sources provides a significant advantage for applications: 10.6 dB higher SNR means that it will take about 130 individual measurements for the ps-SC source to achieve the same quality of data, as just from a *single* measurement with the FOCR source, as follows from the square-root law of error propagation in signal averaging. We note that additional measurements on a similar ps-SC source showed a certain increase in SNR by 2.2 dB, when the bandwidth of the bandpass filter increases from 10 nm to 40 nm at the 600 nm wavelength, which is still significantly higher noise figure as compared to the FOCR source with similar spectral

output. The noise characterization of several different FOCR sources was recently presented by Tu *et al.* in work [57].

As the all-fiber CR lasers do not require any maintenance and demonstrate the option of purely-electrical tunability, we anticipate that the monolithic FOCR laser technology will find wide applicability in practical biophotonics and biomedical applications.

#### 4. Applications and prospects

The applications in biophotonics and biomedical imaging are the primary driving force for the development of FOCR-based fiber lasers. For example, Chan *et al.* have recently demonstrated the successful use of FOCR in nonlinear light microscopy (NLM) [35] and optical coherence tomography (OCT) [58].

To demonstrate the feasibility of femtosecond FOCR as a nonlinear microscopy light source, several bio-samples have been studied using the FOCR laser source by Chan *et al.* in [35]. Due to the compactness of the FOCR light source, the output of the FOCR laser with a 120 mW average power and a 700 nm central wavelength was directly connected to the nonlinear microscope without any external pulse compression components. Sectioned two photon fluorescence (TPF) images from a mouse brain blood vessel network (Fig. 13(a) and (b)), and second harmonic generation (SHG) images of rat tail tendon (Fig. 13(c)) were obtained. The results indicated that the image performance based on the FOCR source was comparable to that based on commercially available Ti:Sapphire lasers in the 0.6–0.8  $\mu\text{m}$  wavelength regime. This preliminary demonstration in NLM shows that the compact FOCR source with fiber-end pulse delivery can indeed potentially be utilized for clinical diagnostics. Moreover, endoscopic imaging is within reach, since the FOCR output is perfectly compatible with fiber-based endoscope systems.

As a multispectral light source, FOCR was used for spectral-domain optical coherence tomography (SD-OCT) applications [58]. The output spectral range of this multispectral light source was composed of 0.6–0.9  $\mu\text{m}$  blue-shifted FOCR, 1.0  $\mu\text{m}$  residual pump, and 1.1–1.7  $\mu\text{m}$  red-shifted soliton self-frequency shifted (SSFS) signal with more than 1 mW/nm power spectral density. The light source was then connected to an SD-OCT system, and successful SD-OCT imaging of an IR card and finger skin was performed. The plastic plate and particles of phosphorus were successfully identified from the 2D and 3D OCT results of the IR card, and the epidermis and dermis were observed from the *in vivo* OCT results of the fingertip and finger skin. These results indeed indicate that due to the advantages of simplicity, ease of operation, and wavelength tunability, the CR fiber laser sources are widely applicable for various real-life biophotonics and biomedical applications.

We note that all the aforementioned laser systems are the result of direct use of the FOCR mechanism to generate specific NIR, VIS and UV short-wavelengths from NIR pump sources via optical frequency up-conversion. However, as we already discussed in Section 2, FOCR mechanism also allows for the complementary possibility of FOCR generation on the long-wavelength side of the soliton via frequency down-conversion [59], [60]. Efficient frequency conversion from a 1064 nm sub-nanosecond pulse pump to FOCR centered at

~1535 nm in a microstructured double core fiber was reported in [61]. Our recent theoretical work [15] has shown that the generation of MIR FOCR light in the 3–4  $\mu\text{m}$  wavelength range is also feasible with existing silica-based PCFs. The FOCR up to 3.5  $\mu\text{m}$  can be generated in a short (a few centimeters) piece of silica PCF pumped by one 1.5  $\mu\text{m}$  fs laser source, and the FOCR in the 3.5–4  $\mu\text{m}$  range in an efficient manner can be generated in even shorter (sub-cm) PCF lengths. This generated MIR wavelength range is of especially high interest for spectroscopy, imaging, and femtochemistry because of the presence of important fundamental stretching vibrations e.g., from O-H, N-H, and C-H chemical bonds. IR FOCR system will further expand an already broad field of application of this new technology.

## 5. Conclusions

In this work, we reviewed the basic principles and recent developments in the field of ultrafast Cherenkov fiber lasers. The state-of-the-art FOCR laser systems offer wide wavelength tunability, such as across the entire NIR, VIS and UV range, and high pump-to-CR power conversion efficiency often exceeding 40%. At the same time, the FOCR mechanism also permits efficient pump down-conversion and hence the emission in the MIR range. The FOCR generation is inherently tolerant to the pump pulse shape, permitting the use of simple, un-optimized lasers as the pump sources. A robust, all-fiber architecture of femtosecond CR source provides for the ease of integration with bio-imaging application platforms. Such a solution offers a very high mechanical stability and very low intensity noise level, which is again highly advantageous for microscopy applications. Current effort in the field of FOCR is in particular concentrated on increasing the pump-to-CR conversion efficiency along a broader spectral range, and the development of widely continuously tunable all-fiber FOCR lasers.

## Acknowledgments

We acknowledge the Danish Council for Independent Research - Technology and Production Sciences (FTP project ALFIE), European Commission (EU Career Integration Grant 334324 LIGHTER), and the National Institutes of Health, National Cancer Institute (1 R01 CA166309) for financial support; and NKT Photonics A/S for providing the PCFs.

## References

1. Tu H, Boppart SA. Ultraviolet-visible non-supercontinuum ultrafast source enabled by switching single silicon strand-like photonic crystal fibers. *Opt Express*. 2009; 17:17983–17988. [PubMed: 19907587]
2. Savage N. Optical parametric oscillators. *Nature Photon*. 2010; 4:124–125.
3. Dunn M, Ebrahimpzadeh M. Parametric generation of tunable light from continuous-wave to femtosecond pulses. *Science*. 1999; 286:1513–1517. [PubMed: 10567249]
4. Dudley JM, Genty G, Coen S. Supercontinuum generation in photonic crystal fiber. *Rev Mod Phys*. 2006; 78:1135–1184.
5. Lison, F.; Hellerer, T. Tunable laser sources: fully tunable visible laser source is valuable for biophotonics. *Laser Focus World*; 2009.
6. Price JHV, Monro T, Ebendorff-Heidepriem H, Poletti F, Horak P, Finazzi V, Leong JYY, Petropoulos P, Flanagan J, Brambilla G, Feng X, Richardson David J. Mid-IR supercontinuum generation from nonsilica microstructured optical fibers. *IEEE J Sel Top Quantum Electron*. 2007; 13:738–749.

7. Dudley, JM.; Taylor, JR., editors. Supercontinuum generation in optical fibers. Cambridge University Press; 2010.
8. Bolotovskii BM, Ginzburg VL. The Vavilov-Cerenkov effect and the Doppler effect in the motion of sources with superluminal velocity in vacuum. *Sov Phys Usp.* 1972; 15:184–192.
9. Wai PKA, Menyuk CR, Lee YC, Chen HH. Nonlinear pulse propagation in the neighborhood of the zero-dispersion wavelength of monomode optical fibers. *Opt Lett.* 1986; 11:464–466. [PubMed: 19730665]
10. Akhmediev N, Karlsson M. Cherenkov radiation emitted by solitons in optical fibers. *Phy Rev A.* 1995; 51:2602–2607.
11. Agrawal, GP. Nonlinear fiber optics. 4. Academic Press; 2007.
12. Gordon JP. Dispersive perturbations of solitons of the nonlinear Schrödinger equation. *J Opt Soc Am B.* 1992; 9:91–97.
13. Cristiani I, Tediosi R, Tartara L, Degiorgio V. Dispersive wave generation by solitons in microstructured optical fibers. *Opt Express.* 2004; 12:124–135. [PubMed: 19471518]
14. Elgin JN, Brabec T, Kelly SMJ. A perturbative theory of soliton propagation in the presence of third order dispersion. *Opt Commun.* 1995; 114:321–328.
15. Lægsgaard J, Tu H. How long wavelengths can one extract from silica-core fibers? *Opt Lett.* 2013; 38:4518–4521. [PubMed: 24177134]
16. Herrmann J, Griebner U, Zhavoronkov N, Husakou A, Wadsworth WJ, Knight JC, St Russell PJ, Korn G. Experimental evidence for supercontinuum generation by fission of higher-order solitons in photonic fibers. *Phys Rev Lett.* 2002; 88:173901 1–4. [PubMed: 12005754]
17. Lægsgaard J, Bjarklev A, Barkou Libori SE. Chromatic dispersion in photonic crystal fibers: fast and accurate scheme for calculation. *J Opt Soc Am B.* 2003; 20:443–448.
18. Johnson SG, Joannopoulos JD. Block-iterative frequency-domain methods for Maxwell's equations in a planewave basis. *Opt Express.* 2001; 8:173–190. [PubMed: 19417802]
19. Svane, AS. PhD Dissertation. Technical University of Denmark; Nonlinear frequency conversion in fiber lasers.
20. Hu M, Wang CY, Chai L, Zheltikov A. Frequency-tunable anti-Stokes line emission by eigenmodes of a birefringent microstructure fiber. *Opt Express.* 2004; 12:1932–1937. [PubMed: 19475026]
21. Mitrofanov AV, Linik YM, Buczynski R, Pysz D, Lorenc D, Bugar I, Ivanov AA, Alifimov MV, Fedotov AB, Zheltikov AM. Highly birefringent silicate glass photonic-crystal fiber with polarization-controlled frequency-shifted output: A promising fiber light source for nonlinear Raman microspectroscopy. *Opt Express.* 2006; 14:10645–10651. [PubMed: 19529469]
22. Lu F, Deng Y, Knox WH. Generation of broadband femtosecond visible pulses in dispersion-micromanaged holey fibers. *Opt Lett.* 2005; 30:1566–1568. [PubMed: 16007809]
23. Amorim AA, Crespo HM, Miranda M, Silva JL, Bernardo LM. Study of non-solitonic blue-green radiation generated in mm-long photonic crystal fibres. *Proc of SPIE.* 2006; 6187:618717.
24. Lu F, Knox WH. Generation, characterization, and application of broadband coherent femtosecond visible pulses in dispersion micromanaged holey fibers. *J Opt Soc Am B.* 2006; 23:1221–1227.
25. Tu H, Boppart SA. Optical frequency up-conversion by supercontinuum-free widely-tunable fiber-optic Cherenkov radiation. *Opt Express.* 2009; 17:9858–9872. [PubMed: 19506636]
26. Tu H, Boppart SA. Versatile photonic crystal fiber-enabled source for multi-modality biophotonic imaging beyond conventional multiphoton microscopy. *Proc SPIE 7569.* 2010:75692D.
27. Tu H, Boppart SA. Coherent fiber supercontinuum for biophotonics. *Laser Photon Rev.* 2013; 7:628–645.
28. Joly NY, Nold J, Chang W, Hölzer P, Nazarkin A, Wong GKL, Biancalana F, St Russell PJ. Bright spatially coherent wavelength-tunable deep-UV laser source using an Ar-filled photonic crystal fiber. *Phys Rev Lett.* 2011; 106:203901-1–4. [PubMed: 21668228]
29. Mak KF, Travers JC, Hölzer P, Joly NY, St Russell PJ. Tunable vacuum-UV to visible ultrafast pulse source based on gas-filled Kagome-PCF. *Opt Express.* 2013; 21:10942–10953. [PubMed: 23669950]
30. St Russell PJ, Hölzer P, Chang W, Abdolvand A, Travers JC. Hollow-core photonic crystal fibres for gas-based nonlinear optics. *Nat Photonics.* 28:278–286.

31. Tu H, Lægsgaard J, Zhang R, Tong S, Liu Y, Boppart SA. Bright broadband coherent fiber sources emitting strongly blue-shifted resonant dispersive wave pulses. *Opt Express*. 2013; 21:23188–23196. [PubMed: 24104233]
32. Chang G, Chen LJ, Kärtner FX. Highly efficient Cherenkov radiation in photonic crystal fibers for broadband visible wavelength generation. *Opt Lett*. 2010; 35:2361–2363. [PubMed: 20634830]
33. Yuan J, Sang X, Yu C, Han Y, Zhou G, Li S, Hou L. Highly efficient and broadband Cherenkov radiation at the visible wavelength in the fundamental mode of photonic crystal fiber. *IEEE Photon Technol Lett*. 2011; 23:786–788.
34. Zhang XB, Zhu X, Chen L, Jiang FG, Yang XB, Peng JG, Li JY. Enhanced violet Cherenkov radiation generation in GeO<sub>2</sub>-doped photonic crystal fiber. *Appl Phys B*. 2013; 111:273–277.
35. Chan MC, Lien CH, Lu JY, Lyu BH. High power NIR fiber-optic femtosecond Cherenkov radiation and its application on nonlinear light microscopy. *Opt Express*. 2014; 22:9498–9507. [PubMed: 24787838]
36. Chang G, Chen LJ, Kärtner FX. Fiber-optic Cherenkov radiation in the few-cycle regime. *Opt Express*. 2011; 19:6635–6647. [PubMed: 21451691]
37. Knight, JC.; Birks, TA.; Atkin, DM.; St Russell, PJ. Pure silica single-mode fiber with hexagonal photonic crystal cladding. *Proc. Opt. Fiber Commun. Conf. No. PD3 post deadline*; 1996;
38. Lin A, Zhang A, Bushong EJ, Toulouse J. Solid-core tellurite glass fiber for infrared and nonlinear applications. *Opt Express*. 2009; 17:16716–16721. [PubMed: 19770886]
39. Cheng T, Deng D, Xue X, Zhang L, Suzuki T, Ohishi Y. Highly efficient tunable dispersive wave in a tellurite microstructured optical fiber. *IEEE Photon J*. 2015; 7:2200107.
40. Liu X, Lægsgaard J, Møller U, Tu H, Boppart SA, Turchinovich D. All-fiber femtosecond Cherenkov radiation source. *Opt Lett*. 2012; 37:2769–2771. [PubMed: 22743523]
41. Liu X, Lægsgaard J, Turchinovich D. Self-stabilization of a mode-locked femtosecond fiber laser using a photonic bandgap fiber. *Opt Lett*. 2010; 35:913–915. [PubMed: 20364167]
42. Liu X, Lægsgaard J, Turchinovich D. Highly-stable monolithic femtosecond Yb-fiber laser system based on photonic crystal fibers. *Opt Express*. 2010; 18:15475–15483. [PubMed: 20720927]
43. Liu X, Lægsgaard J, Turchinovich D. Monolithic highly-stable Yb-doped femtosecond fiber lasers for applications in practical biophotonics. *J Sel Top Quant Electron*. 2012; 18:1439–1450.
44. Turchinovich D, Liu X, Lægsgaard J. Monolithic all-PM femtosecond Yb-fiber lasers stabilized with a narrow-band fiber Bragg grating and pulse-compressed in a hollow-core photonic crystal fiber. *Opt Express*. 2008; 16:14004–14014. [PubMed: 18773011]
45. Li D, Zheng W, Qu JY. Two-photon autofluorescence microscopy of multicolor excitation. *Opt Lett*. 2009; 34:202–204. [PubMed: 19148255]
46. Palero J, Boer V, Vijverberg J, Gerritsen H, Sterenborg HJCM. Short-wavelength two-photon excitation fluorescence microscopy of tryptophan with a photonic crystal fiber based light source. *Opt Express*. 2005; 13:5363–5368. [PubMed: 19498530]
47. Shin S, Sharma U, Tu H, Jung W, Boppart SA. Characterization and analysis of relative intensity noise in broadband optical sources for optical coherence tomography. *IEEE Photon Technol Lett*. 2010; 22:1057–1059.
48. von der Linde D. Characterization of the noise in continuously operating mode-locked lasers. *Appl Phys B*. 1986; 39:201–217.
49. Derickson, D., editor. *Fiber Optic Test and Measurement*. Prentice Hall; 1998.
50. Scott RP, Langrock C, Kolner BH. High-dynamic-range laser amplitude and phase noise measurement techniques. *J Sel Top Quant Electron*. 2001; 7:641–655.
51. Møller U, Sørensen ST, Jakobsen C, Johansen J, Moselund PM, Thomsen CL, Bang O. Power dependence of supercontinuum noise in uniform and tapered PCFs. *Opt Express*. 2012; 20:2851–2857. [PubMed: 22330522]
52. Møller U, Sørensen ST, Jakobsen C, Johansen J, Moselund PM, Thomsen CL, Bang O. Power dependence of supercontinuum noise in uniform and tapered PCFs: erratum. *Opt Express*. 2012; 20:23318–23319.
53. Liu X, Villanueva GE, Lægsgaard J, Møller U, Tu H, Boppart SA, Turchinovich D. Low-noise operation of all-fiber femtosecond Cherenkov laser. *IEEE Photon Technol Lett*. 2013; 25:892–895.

54. Newbury NR, Washburn BR, Corwin KL, Windeler RS. Noise amplification during supercontinuum generation in microstructure fiber. *Opt Lett*. 2003; 28:944–946. [PubMed: 12816254]
55. Corwin KL, Newbury NR, Dudley JM, Coen S, Diddams SA, Weber K, Windeler RS. Fundamental noise limitations to supercontinuum generation in microstructure fiber. *Phys Rev Lett*. 2003; 90:113904. [PubMed: 12688929]
56. Møller U, Sørensen ST, Larsen C, Moselund PM, Jakobsen C, Johansen J, Thomsen CL, Bang O. Optimum PCF tapers for blue-enhanced supercontinuum sources. *Opt Fiber Technol*. 2012; 18:304–314.
57. Tu H, Zhao Y, Liu Y, Liu YZ, Boppart SA. Noise characterization of broadband fiber Cherenkov radiation as a visible-wavelength source for optical coherence tomography and two-photon fluorescence microscopy. *Opt Express*. 2014; 22:20138–20143. [PubMed: 25321223]
58. Tsai MT, Chan MC. Simultaneous 0.8, 1.0, and 1.3  $\mu\text{m}$  multispectral and common-path broadband source for optical coherence tomography. *Opt Lett*. 2014; 39:865–868. [PubMed: 24562227]
59. Skryabin DV, Luan F, Knight JC, St Russell PJ. Soliton self-frequency shift cancellation in photonic crystal fibers. *Science*. 2003; 301:1705–1708. [PubMed: 14500977]
60. Mussot A, Beaugeois M, Bouazaoui M, Sylvestre T. Tailoring CW supercontinuum generation in microstructured fibers with two-zero dispersion wavelengths. *Opt Express*. 2007; 15:11553–11563. [PubMed: 19547513]
61. Manili G, Tonello A, Modotto D, Andreana M, Couderc V, Minoni U, Wabnitz S. Gigantic dispersive wave emission from dual concentric core microstructured fiber. *Opt Lett*. 2012; 37:4101–4103. [PubMed: 23027292]

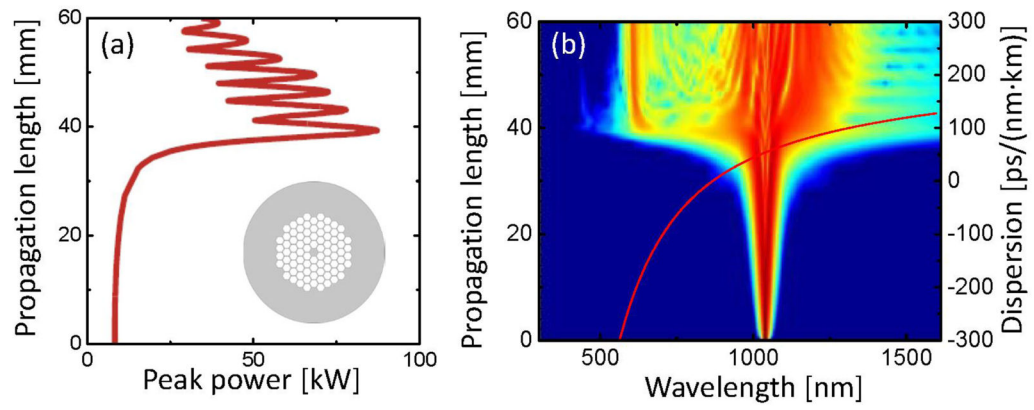


**Figure 1.**

(a) Temporal peak power evolution of the pump pulse along the PCF fiber length. Inset: The representative scanning electron microscopy (SEM) image of the PCF. (b) Colour plot of the output spectrum plotted along the fiber length and dispersion profile of the PCF (red line). Adapted from [19], with permission.

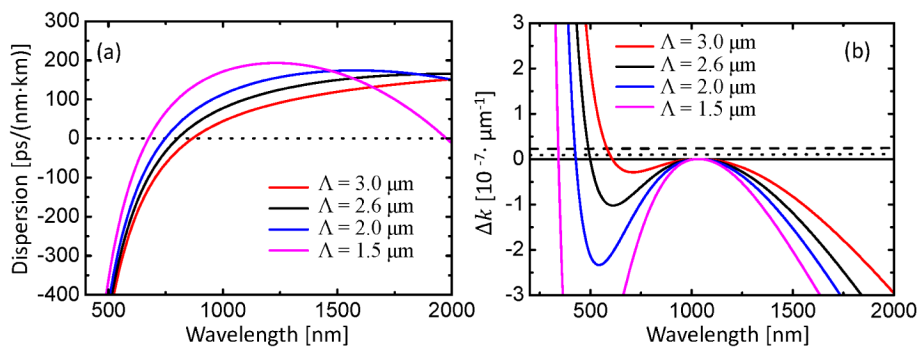


**Figure 2.**

(a) Calculated group velocity dispersion profiles for different fiber dimensions with  $d/\Lambda=0.9$ . (b) Calculated linear FOCR phase-matching curves for different fiber dimensions with  $d/\Lambda=0.9$ , and pump wavelength of 1033 nm; The dotted and dashed lines correspond to the nonlinear induced shift in phase-matching for 50 and 100 kW peak power, respectively. Adapted from [19], with permission.

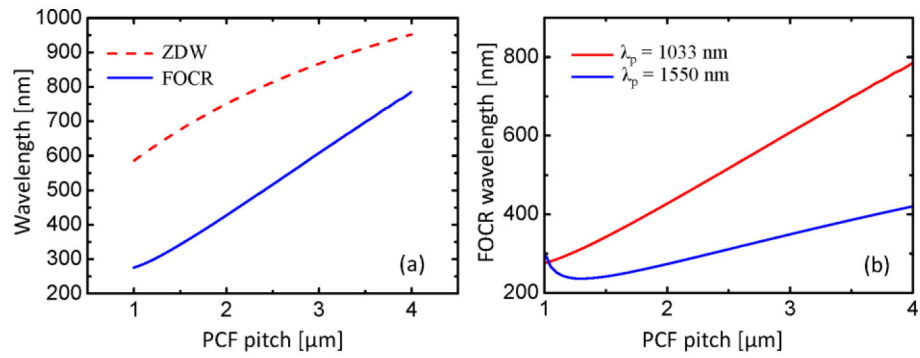


**Figure 3.**

(a) The calculated ZDW (dashed red line) and predicted linear FOCR phase-matching wavelength with a 1033 nm pump wavelength (solid blue line) as a function of the PCF pitch, for  $d/\Lambda = 0.9$ . (b) Predicted linear FOCR phase-matching wavelength with different pump wavelengths for a PCF with a 3  $\mu\text{m}$  pitch. Adapted from [19], with permission.

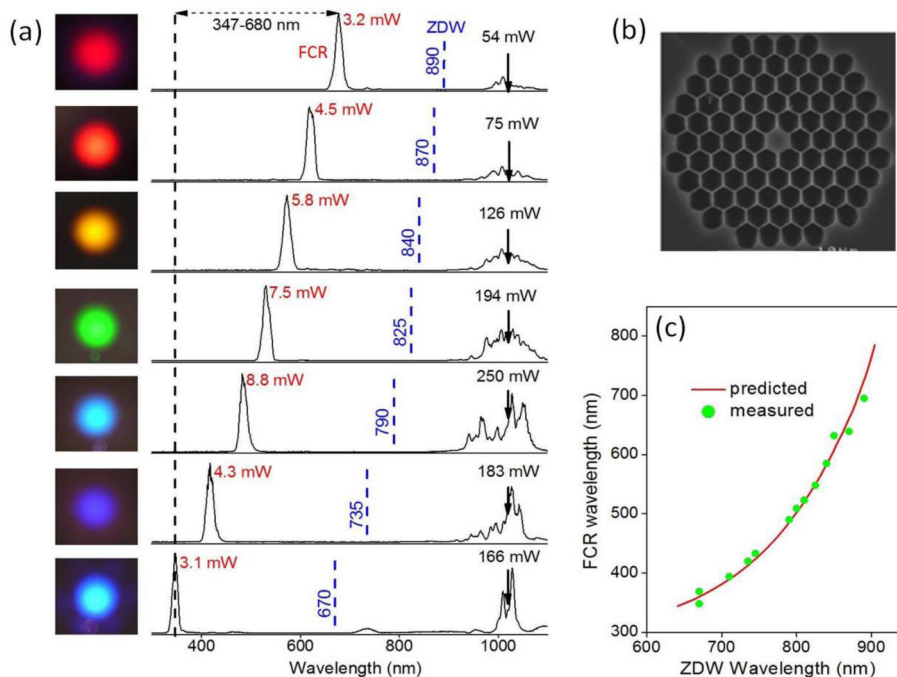


**Figure 4.**

(a) Generation of multi-milliwatt CR from seven different ~10 cm - long PCFs with varying ZDWs (broken vertical lines) by 1020 nm, 170 fs FWHM, 80 MHz input pulses from a Ti:sapphire laser (arrows). Insets: the far-field images of the output light. (b) The representative SEM image of the cross section of the PCFs with varying core size (1.5–3.3  $\mu\text{m}$ ). (c) Comparison of predicted FOCR wavelength as a function of the ZDW of single silica strand (line) according to FOCR phase-matching condition and measured FOCR wavelengths of 13 different single silica strand-like PCFs with varying ZDWs (points). Adapted from [27], with permission.

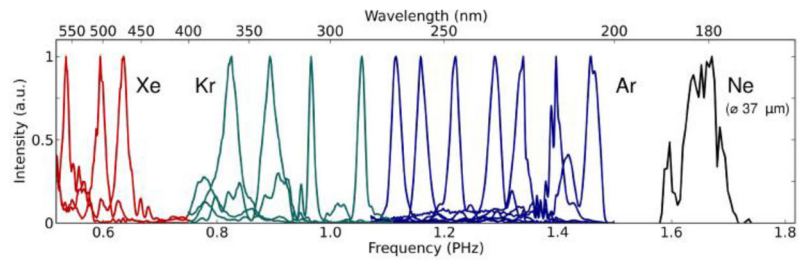


**Figure 5.** Generation of deep-ultraviolet light in gas-filled PCFs pumped at 800 nm: the ultraviolet signal, optimized to be narrow-band, can be tuned from 176 nm to 550 nm by varying the pressure and the gas in the PCF. Adapted from [29], with permission.

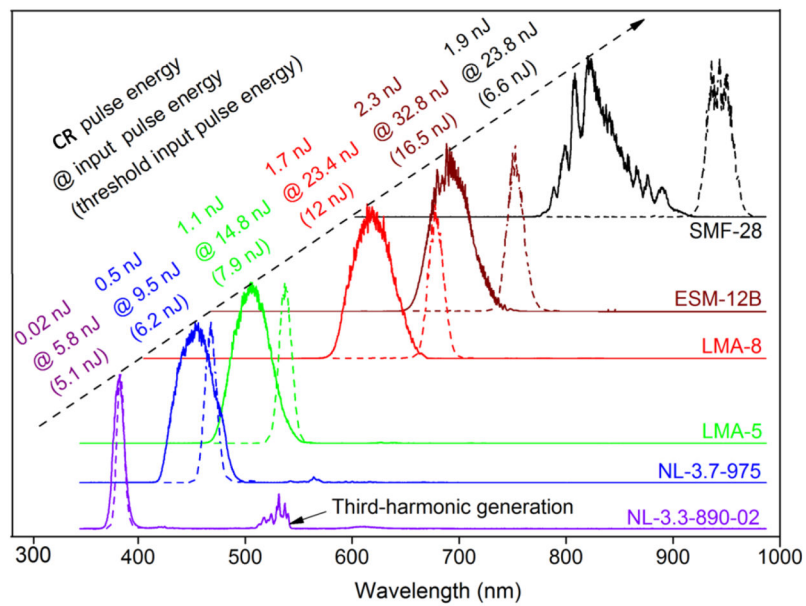


**Figure 6.** The spectra of generated FOCR at threshold input pulse energies (broken curves) and higher input pulse energies (solid curves) from a series of 9 cm nonlinear fibers, along with FOCR pulse energies at the higher input pulse energies, generated by 1550 nm pump pulses. Adapted from [31], with permission.

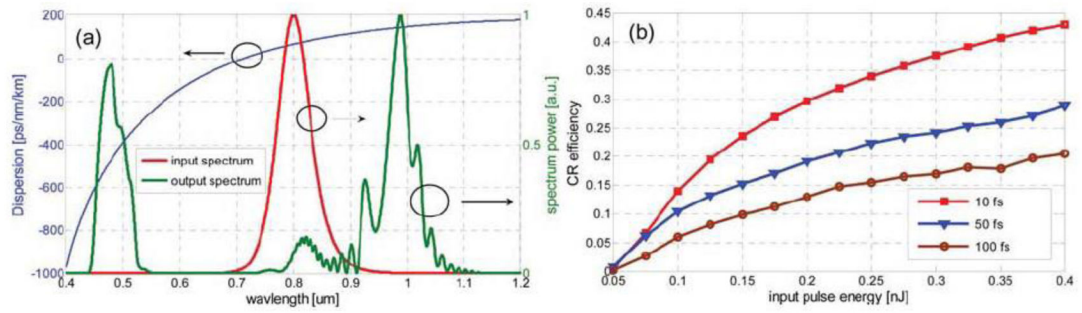


**Figure 7.**

(a) PCF dispersion and calculated pulse spectrum after propagating a 300 pJ, 10 fs pulse through 2 cm PCF and (b) Calculated CR efficiency versus input pulse energy for three FWHM durations of the input pulse: 10 fs, 50 fs, and 100 fs. Adapted from [32], with permission.

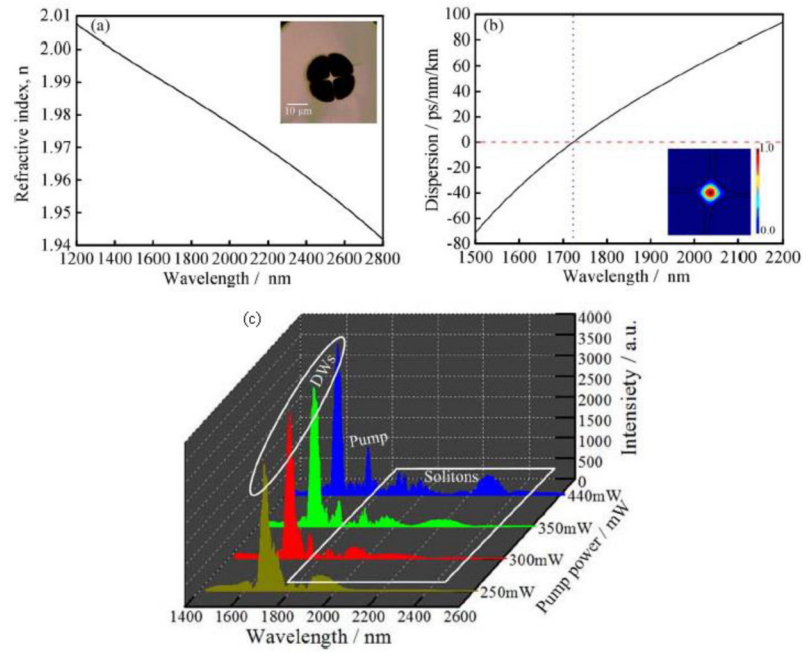


**Figure 8.**

(a) Fundamental mode refractive index of the tellurite microstructured optical fiber (TMOF). Inset: Cross section of the TMOF. (b) Calculated dispersion curve of the fundamental mode. Inset: Fundamental mode-field profile at 1800 nm. (c) FOCR evolution dependent on the average input pump power. Adapted from [39], with permission.

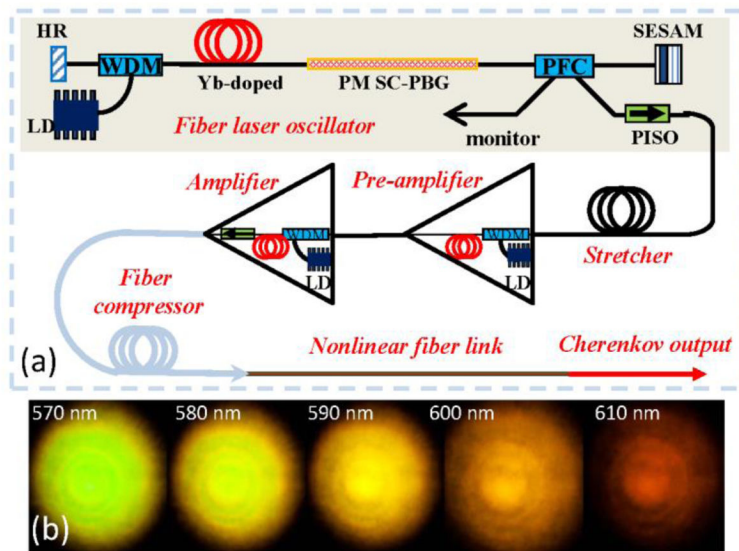


**Figure 9.**

(a) Layout of the all-fiber fs FOCR source: HR -- high-reflectivity pigtailed mirror, WDM -- 980/1030 wavelength division multiplexer, LD -- single-mode pumping diode at 974 nm, PM SC-PBG -- PM all-solid photonic bandgap fiber, SESAM -- semiconductor saturable absorber mirror, PISO -- polarization-maintaining isolator, PFC -- 80/20 polarization filter coupler, Fiber compressor -- hollow-core photonic crystal fiber, Nonlinear fiber link -- highly nonlinear fiber for FOCR generation. (b) Far-field VIS images of the generated Cherenkov output with different central wavelength.

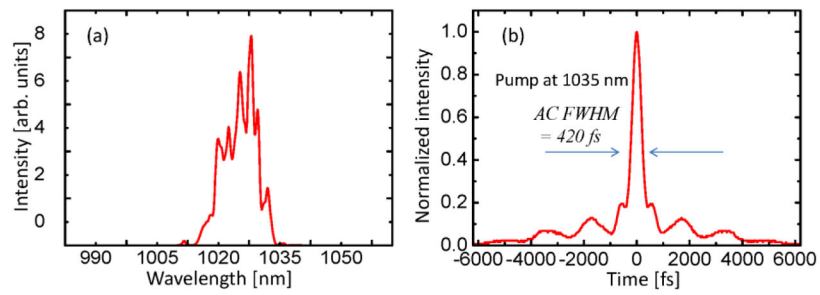


**Figure 10.**

(a) Optical spectra and (b) autocorrelation (AC) of the input femtosecond pump signal. The corresponding emitted FOCR output spectra, measured at different output powers are shown in Fig. 11(a).

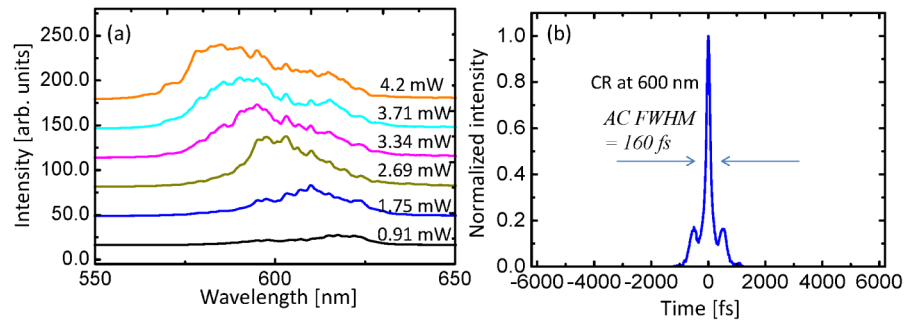


**Figure 11.**

(a) Optical spectra of the generated FOCR dependent on the output power. (b) AC of the generated FOCR with the output power of 1.7 mW. The characteristics of the pump laser are shown in Fig. 10.

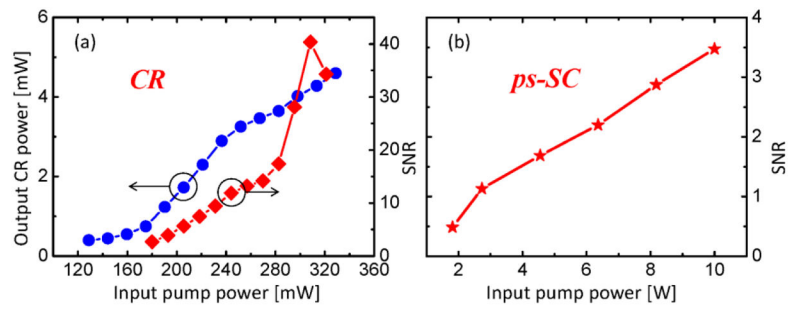


**Figure 12.**

(a) Output power (circles) and SNR (diamonds) of generated FOCR as a function of the input pump power. (b) Comparison with a typical spectrally-sliced supercontinuum source: SNR of the output of a typical all-fiber ps-SC source, spectrally sliced at 600 nm, as a function of the input pump power.

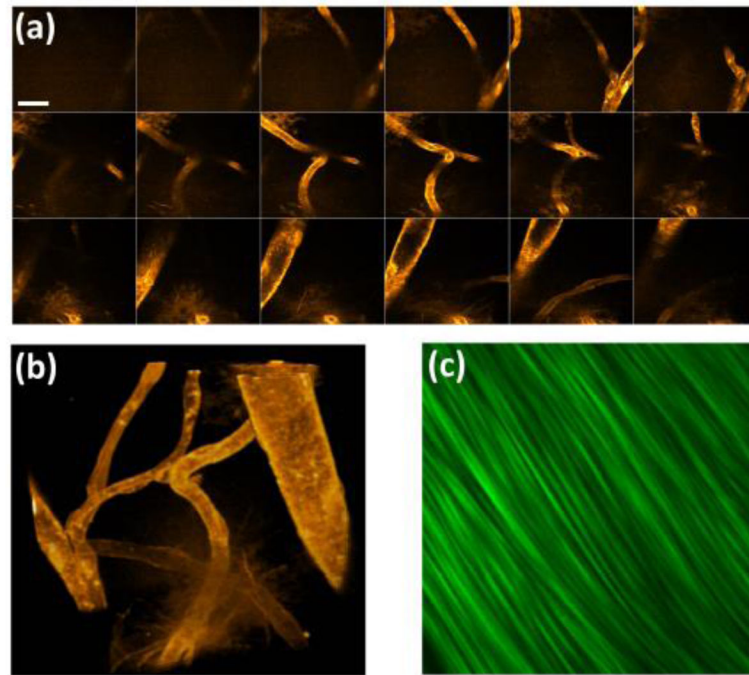


**Figure 13.**

(a) Sectioned two-photon fluorescence images (TPF) of blood vessels in mouse brains with different z depth. The scale bar length is  $25\ \mu\text{m}$  and the z-step size is  $5\ \mu\text{m}$ . (b) Reconstructed 3D blood vessel network in the mouse brain. (c) Second harmonic generation image (SHG) of rat tail tendon in phosphate buffered saline. Image size:  $50\ \mu\text{m}$  by  $50\ \mu\text{m}$ . Adapted from [35], with permission.

Table 1

Representative ultrafast FOCR laser systems.

Pump laser sources		Nonlinear fiber(s)			CR wave.	Eff.	Ref.
Type	Wavelength	Duration	Rep. rate	Type	Length		
Ti:sapphire	800 nm	190 fs	80 MHz	PCF	40 cm	430 nm	25% [13]
Ti:sapphire	820 nm	35 fs	100 MHz	PCFs	10 cm	490 & 510 nm	20% [20]
Cr:forsterite	1.24 $\mu\text{m}$	100 fs	1 KHz	Specific PCFs	8 cm	530–720 nm	1% [21]
Ti:sapphire	880–900 nm	100 fs	80 MHz	PCFs	5–10 cm	538 & 600 nm	20% [22]
Ti:sapphire	800 nm	20 fs	85 MHz	2 PCFs	5 mm	470–500 nm	- [23]
Ti:sapphire	880–900 nm	100fs	80 MHz	Tapered PCF	1–2 cm	385–625 nm	- [24]
Ti:sapphire	690–1020 nm	100 fs	80 MHz	2 PCFs	10 cm	485–690 nm	10% [25]
Ti:sapphire	1020 nm	170 fs	80 MHz	Series PCFs	15–18 cm	347–680 nm	2–6% [1][26], [27]
Ti:sapphire	800 nm	80 fs	50 MHz	Gas-filled HC-PCFs	10–90 cm	176–550 nm	8% [28], [29]
Er: fiber laser	1550 nm	80 fs	50 MHz	Nonlinearity fibers	9cm	370–850 nm	7% [31]
Ti:sapphire	800 nm	10 fs	85 MHz	PCF	2 cm	450–550 nm	40% [32]
Ti:sapphire	800 nm	120 fs	76 MHz	PCF	50 cm	545–580 nm	8–31% [33]
Yb-doped PCF laser	1.038 $\mu\text{m}$	95 fs	49 MHz	Two-ZDW PCF	2 m	410 & 423 nm	40% [34]
Yb-doped laser	1.03 $\mu\text{m}$	250 fs	54.77 MHz	PCF	8.5 cm	670–790 nm	40% [35]
OPO	1.76–1.91 $\mu\text{m}$	560 fs	80 MHz	TMOF	2 cm	1626–1685 nm	65% [39]
All-fiber Yb- doped laser	1.035 $\mu\text{m}$	300 fs	28 MHz	Spliced on PCF	10 cm	580–630 nm	1% [40]